RSC Advances

ROYAL SOCIETY OF CHEMISTRY

www.rsc.org/advances

A comparative study of structure and electromagnetic interference shielding performance for silver nanostructures hybrid polyimide foams

Jingjing Ma*[a], Kai Wang *[a], and Maosheng Zhan*[a]

[a] Key Laboratory of Aerospace advanced materials and performance (Ministry of Education), School of Materials Science and Engineering, Beihang University, Beijing 100191, P.R. China

*Corresponding Author; Email: majingjingbh@126.com or wangkai@buaa.edu.cn or zhanms@buaa.edu.cn; Tel: +86 10 82338557

Abstract: Silver nanofillers of three different shapes were synthesized: silver nanospheres (AgNSs), silver nanowires (AgNWs) and silver nanowires-silver nanoplatelets (AgNWPs). Ultra-lightweight polyimide (PI) composite foams filled with these three silver nanofillers were fabricated by a facile and effective one-pot liquid foaming process, respectively. Their microstructure, electromagnetic interference (EMI) shielding effectiveness (SE) and shielding mechanisms were investigated. It was found that, at the same nanofiller loading, the EMI SE of the composite foams decreased in the following order: AgNWPs > AgNWs > AgNSs. AgNWPs/PI composite foams exhibited the highest EMI SE owing to the denser 3D conductive network of AgNWPs compared to AgNWs and AgNSs, in which the interconnected seamlessly AgNWPs network provided fast electron transport channels inside foams. A maximum specific EMI SE of 1208 $dB \cdot g^{-1} \cdot cm^3$ at 200 MHz, 650 $dB \cdot g^{-1} \cdot cm^3$ at 600 MHz, and 488 $dB \cdot g^{-1} \cdot cm^3$ in the frequency range of 800-1500 MHz, 216-249 $dB \cdot g^{-1} \cdot cm^3$ at 8-12 GHz were achieved in composite foams at 4.5 wt% AgNWPs loading, which far surpasses the best values of other composite materials. The reflections of interconnected AgNWPs networks inside foams combined with absorptions resulting from the multiple reflections at interfaces inside foams contributed to the shielding effect. This suggests that our AgNWPs/PI composite foam has excellent potential as high-performance EMI shielding materials against electromagnetic interference pollution in applications that need lightweight.

1. Introduction

Recently, the rapidly increasing usage of transient power sources and the extensive development of modern electronics packed with integrated circuits have resulted in serious electromagnetic interference (EMI) pollution, which affected sensitive electronic instruments and the health of human beings adversely.[1-3] Thus, considerable attentions have been devoted to the development of high-performance EMI shielding materials.[4-6] Electrically conductive polymer composites made of conductive nanoparticles dispersed in polymer matrixes are excellent candidates for preparing lightweight EMI shielding materials because they exhibit low density, high processing ability, tunable conductivity, and resistance to corrosion compared to metal-based EMI shielding materials.[7-15] The common conductive nanofillers are composed of carbon-based nanoparticles like carbon nanofibers(CNFs)[7], carbon nanotubes (CNTs)[8-10] and graphene nanoplatelets,[11-15] and metal-based nanoparticles like stainless-steel fiber,[16] Cu nanowires,[17] silver nanowires (AgNWs)[18,19] and silver nanoplates.[20] It has been demonstrated, at the same carbon-based nanofiller loading, the composites filled with high aspect ratio CNTs displayed higher EMI shielding effectiveness (SE) than composites filled with low aspect nanofillers such as CNFs at 8-12 GHz,[21-23] which played an important role in designing composites for high-performance EMI shielding. It is well known that higher the electrical conductivity of composites, the higher their EMI SE. However, in the case of conductive polymers, carbon-based fillers, the conductivity is 2-4 orders of magnitude lower than that of metal nanotructures.[24] We believed that metal nanostructures are promising nanofillers for polymer composites as EMI shielding materials. In order to develop polymer composites for high-performance EMI shielding, it is very essential to compare the EMI SE of polymeric materials filled with metal nanostructures.

Among all metal nanostructures, silver nanostructures like nanospheres, nanowires, and nanoplatelets exhibit the highest conductivity. And they can be synthesized with high aspect ratios, and their structure, composition, and surface properties can be controlled by the conditions of their

synthesis.[25-27] It has been reported that silver nanospheres (AgNSs) can be used for preparing inkjet printed flexible electronics with high conductivity due to its high conductivity.[24,28] The resistivity of the adhesives filled with AgNSs could be achieved with 2×10^{-4} Ω·cm.[29] Compared to AgNSs, silver nanoplatelets (AgNPs) exhibit higher aspect ratio and surface area.[30,31] It has been demonstrated that the AgNPs filled polymer showed higher conductivity than the AgNSs filled ones due to the decrease in surface contact area.[31] The most promising nanofiller is AgNW because AgNWs exhibited the highest ratio among the three nanofillers.[32] Thus, a lower content of nanowires is required to form interconnected network in the polymer matrix and to achieve the target properties of composites.[33-36] For instance, AgNWs/polystyrene (PS) composites displayed 10^2 S/m at 1 vol% nanofiller loading.[33] AgNWs/polyamide11 exhibited 10^2 S/m at 3 vol% nanofiller loading.[34] Currently, it has been demonstrated that introducing one-dimensional conductive nanowires for bridging between the conductive nanoplatelets materials could enhance its conductivity.[37] Therefore, if silver nanoplatelets could grow on AgNWs surface to obtain silver nanowires-silver nanoplatelets (AgNWPs), a lower content of AgNWPs would endow composites with excellent conductivity due to AgNWs bridging effects. We believe that silver nanostructures will give polymer composites outstanding EMI shielding performance due to their high electrical conductivity. For example, Al‐Ghamdi et al[38] fabricated polyvinyl alcohol(PVA)/10 wt% Ag nanoparticles composite and achieved a EMI SE of 51 dB at 1-12 GHz. Hu et al.[39] developed silicone rubber/Ag-coated cenosphere particle composites that exhibited an EMI SE of above 80 dB for 65 wt% nanofiller loading at 30 MHz-1.5 GHz. Kwon et al.[20] fabricated silver flakes-carbon nanotubes/nitrile butadiene rubber composites that exhibited an EMI SE of 80 dB for 65 wt% nanofiller loading at 30 MHz-1.5 GHz. Hu et al.[18] fabricated poly(ethersulfones) (PES)/AgNWs/ polyester (PET) sandwich-structured film with an EMI SE of 25 dB at 8-12 GHz. Yu et al.[19] prepared AgNWs/epoxy resin composites that showed an EMI SE of 20 dB at 3-17 GHz.

However, it is very difficult to compare and evaluate the EMI SE performance of the

nanocomposite materials filled with metal nanofillers based on the literature data because the EMI SE data varies with many uncontrolled factors such as the thickness of the shielding samples, the frequency at which the EMI shielding performance was carried out, the polymer matrix type, the fabrication method and processing conditions. Thus, it is of the major objectives of this work to provide a direct comparison between polymer composites based on three different silver nanofillers, namely: AgNSs, AgNWs, and AgNWPs.

Additionally, the conventional polymers such as PP,[16] PMMA,[14] PS,[13] and polyurethane (PU)[40] exhibit low heat-resistance, poor flame retardancy and short lifetime, which restrict their use as the EMI shielding materials in advanced fields. By contrast, polyimide foam (PIF),[41-43] a kind of advanced polymer foam, exhibits high temperature resistance, excellent aging resisting, a high glass transition temperature (Tg) of 292 °C, good flame retardancy, and ultra-low density of 0.013-0.024 g/cm^3, which overcomes the defects of conventional polymers. Thus, it is very valuable to select PIF as the polymer matrix to fabricate high-performance EMI shielding materials. Moreover, polyimide (PI) can be used as a kind of adhesives, and it may stick to silver nanofillers tightly so that silver nanofillers could not peel off easily due to the excellent adhesion between PI matrix and metals.[44] In previous work, we have studied AgNWs hybrid polyimide composite foams for high-performance EMI shielding.[45]

In order to understand the effect of silver nanofillers morphology on the EMI SE and further improve the EMI shielding properties of polyimide composite foams, we report a comparative study of EMI SE of polyimide composite foams filled with AgNSs, AgNWs, and AgNWPs. In this study, the composite foams were fabricated by one-pot liquid foaming process under identical conditions. The morphology and the EMI SE at 30 MHz-1.5 GHz and 8-12 GHz of composite foams at various silver nanofillers were investigated. Moreover, the distribution of silver nanofillers in cells and the shielding mechanism were also demonstrated. To the best of our knowledge, few studies have declared the direct comparison between polymer composites based on these three different silver

nanofillers. This study will lay a foundation of production of high-performance EMI shielding materials used in the advanced fields.

2. Experimental section

2.1 Materials

$AgNO_3$, NaCl, $FeCl_3 \cdot 6H_2O$, acetone and ethanol were all supplied by Beijing Finechem, China. Ethylene glycol (EG) and polyvinylpyrolidone (PVP, Mw≈40000) were purchased from Xilong Chemical Industry Incorporated Co. Ltd., China. 3,3',4,4'-benzophenonetetracarboxylic dianhydride (BTDA) was acquired from Beijing Multi Technology Co. Ltd., China, and was dried in a vacuum oven at 180 ℃ for 8-10 h prior to use. Polyaryl polymethylene isocyanate (PAPI, PM-200) was obtained from Yantai Wanhua Polyurethanes Co. Ltd., China. Silicone oil (DC-193) was purchased from Foshan Daoning Chemical Co. Ltd., China, and it was the main surfactant. Polyethylene glycol 600 (PEG-600), N, N'-dimethylformamide (DMF), methanol and deionized water were also all supplied by Beijing Finechem, China. All chemicals were analytical grade and used without further purification.

2.2 Synthesis of silver nanostructures

Synthesis of AgNSs and AgNWs. AgNSs and AgNWs have been synthesized through the two-step dropping polyol process by simple adjustments of reaction conditions according to our previous technique.[46] AgNSs were synthesized with aid of $FeCl_3$. In the typical synthesis procedure, 40 mL of 0.56 M PVP solution in EG was heated to 160 °C until the temperature was steady. Afterward, 200 μL of 0.05 M $FeCl_3$ solution in EG was injected in the mixture above. Then 10 mL of 1.5 M $AgNO_3$ solution in EG was added into the dropping funnel and then dropped into the flask at the rate of 15 μL/s at first. Once the reaction solution turned to gray which indicated the presence of silver nanoparticles, all the remaining $AgNO_3$ solution was added into the flask immediately. After 2 h, the

reaction was quenched and the suspension was diluted with ethanol (in a weight ratio of 1:10) and centrifuged three times at 8000 rpm for 20 min. The final products were dispersed in DMF and stored at room temperature for further use**.** Uniform AgNWs were synthesized by the same two-step dropping polyol process with aid of NaCl, as previously reported by our group.[45,46] The final products were also dispersed in DMF and stored at room temperature for further use.

Synthesis of AgNWPs. AgNWPs were synthesized by two-step process. Firstly, AgNWs were synthesized as seeds by the two-step dropping polyol process above. Secondly, 16 mL of 0.1875 M PVP solution in DMF was heated to 140 °C in an oil bath until the temperature was steady. Afterward, 2 mL of a DMF solution of Ag seed involving 0.1 mmol of AgNWs was dropped into the mixture above under N_2. Then 12 mL of 0.375-1.5 M $AgNO_3$ solution in DMF was added into the dropping funnel and then dropped into the flask. After 2 h, the reaction was quenched and the suspension was diluted with ethanol and centrifuged at 8000 rpm for 20 min. The precipitates were collected and then redispersed in DMF and stored at room temperature for further use.

2.3 Preparation of silver nanostructures hybrid polyimide composite foams

Silver structures/polyimide in-situ hybrid composite foams were prepared by one-pot liquid foaming process according to our previous technique.[45] First, a predetermined amount of silver nanofillers (AgNSs, AgNWs, AgNWPs) were dispersed in 100 pphp (parts per hundred parts of anhydride by weight) of DMF using a bath sonicator for 60 min in order to achieve optimum dispersion and extensive surface contact with polymer matrix**.** The silver nanofillers solution was then added to a 250 mL flask under N_2 at approximately 85 °C. Afterwards, 100 pphp of BTDA, 40 pphp of processing aids (methanol, DC-193 and PEG-600) and 13 pphp of deionized water were accurately weighted and added to the mixture above. The mixture was stirred for 2 h to give a homogeneous solution named as first solution containing silver nanofillers. When the first solution was cooled to 25 °C, 200 pphp of PAPI was added to the first solution. The mixture of first solution and PAPI was stirred with a high speed mixer (about 2000 rpm) for 5-15 s. Then it was immediately transferred to a

mould where it was allowed to rise freely for 5 min. Once the foam was no longer tacky, it was placed in a vacuum oven at 250 ℃ to posture for 2 hours in order to complete the imidization reaction. High-temperature treatment also could promote effective connections between silver nanofillers. In this experiment, the silver nanofillers loadings were 13 pphp. And they were identified as PIF-P (AgNSs hybrid foam), PIF-W (AgNWs hybrid foam), and PIF-WP (AgNWPs hybrid foam), respectively. Pure PIF named PIF-0 was also fabricated as the comparative test. The chemical reaction that might occur during the preparation was similar to that of our previous study.[43]

2.4 Characterization

The morphology of samples was carried out with a field-emission scanning electron microscope (FESEM, JSM 7500, JEOL) operated at an accelerating voltage of 5 kV after sputter-coating specimens with platinum. The chemical composites were analyzed with an energy dispersive analyzer (EDS, Oxford Inca). The sizes of the silver nanostructures were determined by measuring the sizes of 100 nanostructures from the FESEM images with the aid of SISAC-IAS image analyzer. And the diameters of cells were determined by individually measuring the sizes of 30 cells from the FESEM images. Results are given as averages with standard deviations. The transmission electron microscope (TEM) images were obtained from a JEM-2100 operated at 200 kV. X-ray powder diffraction (XRD) was taken by a D/max 2200 PC X-ray diffractometer operated at a voltage of 40 kV and a current of 40 mA with Cu Kα radiation (λ = 0.15406 nm) at a scanning rate of $0.02°s^{-1}$ in 2θ ranging from 20° to 80°. X-ray photoelectron spectroscopy (XPS) was performed with an ESCALab 250 electron spectrometer from ThermoFisher Scientific USA using 150 W Al Kα radiation. The foam density was measured as the sample weight divided by its volume according to ASTM D328. The results were the average with standard deviation of at least five different foam samples for each composite foam. The open cell content of composite foams was measured by a picnometer (3H-2000TD-K, BeiShiDe Instrument S&T Co. Ltd) according to ASTM D6226. Samples were cut into a cuboid (5cm×2.5cm×2.5cm) to fit a steel container. The reported results

were the averages with standard deviations of three tested samples for each composite foam. The apparent viscosity of first solution was measured using a digital viscometer (NDJ-8S, Shanghai Nirun Intelligent Technology Co. Ltd.) at 25 °C. EMI SE was measured at room temperature in the frequency range of 30 MHz-1.5 GHz according to ASTM D4935-2010 using the standard coaxial cable method. The setup included a DN 1015A SE tester with its input and output connected to an Agilent 8753ES network analyzer which is similar as described in previous study.[47] The samples were cut to disk with diameter of 115 mm to fit the waveguide sample holder. And EMI SE in the X-band frequency of 8-12 GHz was used an Agilent N5242A vector network analyzer (VNA). The VNA was calibrated for the full two-port measurement of reflection and transmission at each port. The samples in rectangle plates with a dimension of 22.5 × 10.0 mm^2 was placed between two X-band waveguide parts that were connected to separate ports of the VNA. Measurement of SE is calculated from scattering parameter S_{ij} which represents the power transmitting from port i to port j. In this two-port network analysis system, the SE can be obtained from the measured S_{11} (or S_{22}) and S_{21} (or S_{12}) parameters. The thickness of all samples was about 5 mm. Volume electrical conductivities below 10^{-6} S/m were measured using a ZC-36 high-resistance meter. The reported results were the averages of five tested samples for each composite foam.

3. Results and discussion

3.1 Structural characterization of silver nanostructures

The as-synthesized silver nanostructures were characterized by FESEM, and the corresponding micrographs of AgNSs and AgNWs are displayed in Fig. 1a and 1b, respectively. As shown in Fig. 1a, the diameter of nanospheres varied from 121 to 175 nm with a mean of 142 nm. And the average diameter and length of nanowires were found to be 90 nm and 7.1 μm (seen Fig. 1b), respectively. In order to investigate the proper condition for the in-situ growth of AgNPs on AgNWs, a series of experiments varying in $AgNO_3$ concentration were carried out. FESEM images of the as-synthesized products synthesized with $AgNO_3$ concentration of 0.15 M, 0.3 M, 0.45 M, and 0.6 M while

maintaining the other parameters constant, are displayed in Fig. 2 (Left: a1-d1), respectively. It is clearly observed that polygon AgNPs grow on the side edges of AgNWs from all the FESEM images. To further understand morphology details of the as-synthesized products, representative TEM images of them are shown in Fig. 2 (Right: a2-d2). When the $AgNO_3$ concentration was 0.15 M, trapezoid platelike flags are grown up from side position of some AgNWs. When the $AgNO_3$ concentration was increased to 0.3 M, the growth rate of nanoplatelets increased more rapidly, and some trapezium flags were grown up to equilateral triangular flags. Further increasing the $AgNO_3$ concentration from 0.3 M to 0.45 M, in addition to equilateral triangular flags, a large number of big irregular polygon nanoplatelets began to grow on AgNWs, leading to the effective bridging effect and interconnection for AgNWs. Excess amount of $AgNO_3$, 0.6 M, made irregular polygons change to pyramidal structures on AgNWs. And a large amount of single spherical nanoparticles were also observed, as depicted in Fig. 2(e1). Our data indicated that 0.45 M $AgNO_3$ concentration was appropriate condition for the in-situ growth of AgNWs on AgNWs to produce AgNWPs at 3 mM AgNWs concentration.

The crystalline nature of the AgNWPs was also identified by XRD techniques shown in Fig. 3a. The as-synthesized AgNWPs exhibited face-centered-cubic (FCC) crystal structure (JCPDS File 04-0783), and the lattice constant calculated from this XRD pattern according to the lattice spacing of the (111) planes was 4.102 Å, which was very close to the reported data value of 4.0862 Å.[45,46] Fig. 3b and 3c shows the XPS spectrum for the Ag 3d and O 1s spectra of the AgNWPs. The spectrum with two peaks at ~367.6 and 373.6 eV corresponding to $3d_{3/2}$ and Ag $3d_{5/2}$ respectively, confirms the presence of metallic silver.[48] Specially, the peak attributed to O 1s is shifted toward higher binding energy (532.0 eV) compared with pure PVP (530.3 eV).[49] The positively shifted O 1s binding energy results from the weakness of electron density around O atoms in the carbonyl group of PVP, indicating that the surfaces of AgNWPs strongly coordinate with O atoms in PVP. Thus, the coordination interaction of PVP on the surface of AgNWPs will promote effective interactions

between AgNWPs and polymer matrix.

On the basis of FESEM and TEM images, we can deduce the in-situ formation mechanism of AgNPs on the surface of AgNWs. It is well known that AgNWs evolved from multiple decahedral particles so that five twin planes exist in nanowires.[46] The driving force of the present shape evolution is the difference in favorable planes in EG and DMF due to selective adsorption of PVP on (100) and (111) planes, respectively. AgNWs with (100) planes are formed preferentially in EG, whereas favorable planes of silver nanostructures in DMF are (111) planes.[50] PVP molecules interacted with silver particles through the oxygen atom in carbonyl and were tightly absorbed on the (100) planes of AgNWs according to the surface-energy minimization.[51] It is believed that these carbonyl functional groups could provide nucleation points for the formation of silver nanoplatelets.[49] Then AgNPs grow on AgNWs surface until the reagents are used up. Thus, twin silver triangular plates surrounded by two wide top and bottom (111) planes and four narrow side (111) planes are formed. And then AgNWPs were obtained. In-situ growth mechanism of the AgNPs on the AgNWs surface is shown in Fig. 4.

3.2 Morphology characterization of silver nanofillers/PI composite foams

The obtained silver nanofillers/PI composite foams are lightweight, as shown in Fig. 5. Judging from the appearance, there were no foaming slags and silver nanofillers peeling off from PI matrix among all the composite foams. The addition of silver nanofillers made the following color changes be noticed: yellow for pure PIF, to pale brown for AgNSs/PIF, to dark yellow for AgNWs/PIF, to green yellow for AgNWPs/PIF at the same nanofiller loading. Table 1 shows the density of silver nanofillers/PI composite foams and their actual nanofillers loading in this study. As shown in Table 1, the density of pure PIF was 0.014 g/cm^3. And the density of AgNWs/polyimide composite foams was 0.015-0.017 g/cm^3, suggesting that the introduction of silver nanofillers didn't change the weight of the composite foams significantly. Our data indicated that silver nanofillers/polyimide composite foams were ultra-lightweight, which effectively meet the requirement of lightweight for effective and

practical shielding applications.

Fig. 6 shows the cell morphology of silver nanostructures/PI composite foams at the same nanofiller loading. Their apparent viscosity of first solution, average cell diameter, and open cell content are summarized in Table 1. The unloaded PI foams exhibited a uniform microcellular structure with average cell size of 397 μm. The addition of silver nanospheres decreased the average cell size to 166 μm for AgNSs loading of 4.5 wt%. With a variation in the silver nanofillers morphology, however, the average cell size tended to increase to 434, 426 μm for AgNWs and AgNWPs at the same nanofiller loading, respectively. This behavior was considered to be due to the effects of nanofillers addition on nucleation and cell growth in the reactive free-rising foaming system.[52-54] In our experiment, silver nanofillers displayed a two-fold role. On one hand, they acted as nucleating agents and promoted the cell nucleation due to the significant reduction in the required energy for creating cells.[55] On the other hand, they increased the apparent viscosity of first solution (Table 1) because of the direct contacts between silver nanofillers and polymer chains.[56] In polyimide composite foam filled with AgNSs, a good dispersion of silver nanofillers in the first solution increased significantly the first solution viscosity (1692 mPa·s), which hindered the cell growth. Meanwhile, a large amount of silver nanospheres promoted the formation of more nucleation sites for cell formation, resulting in a larger number of cells growing to a smaller size. It was also found that the cell size displayed a broad distribution, possibly ascribed to the coalescence effects during the cell growth at this nanofiller loading.[56] As for PIF filled with AgNWs and AgNWPs, a variation in nanofillers morphology from nanospheres, nanoplatelets to nanowires decreased the number of nanofillers for a given nanofiller weight, thereby decreasing the number of final bubbling nucleation sites. At the same time, the viscosity of first solution decreased (924 mPa·s for PIF-W, 976 mPa·s for PIF-WS), however, they were both higher than that of pure PIF (489 mPa·s). As a consequence, the nucleation rate tended to be lower than the cell growth rate, leading to the bigger cell size and inhomogeneous cell distribution. Moreover, the increased pressure inside the small cells

ruptured their cell walls, and they coalesced with adjacent large cells to become larger cells.[56] In addition, it was found that the open cell content decreased slightly from 92.5% to 89.2% with the variation in nanofillers morphologies from AgNSs, AgNWPs to AgNWs. This indicated that silver nanofillers did not promote cell opening during cell growth and hence did not cause the loss of blowing gas. This should be due to the fact that the introduction of rigid silver nanofillers lowered polymer chain flexibility and increased the strength of cell membranes.[57] This highly porous structure gave the composite foams ultralow densities. And the introduction of large volumes of air into the composite foams could limit the mismatch between the wave impedances for the signal propagating in the air and into the shied.[10] Moreover, the presence of micro-cells created a huge gas-solid interface, which was effective for absorptions of electromagnetic waves resulting from multiple reflections.

FESEM was used to investigate the distribution of silver nanofillers in cell structure, and the results are displayed in Fig. 7. As indicated in Fig. 7 (Middle) with magnification of ×1000, cell walls of adjacent micro-cells created triangular cell conjunction. It can be observed that the call walls became thicker with the variation in nanofillers from nanospheres, AgNWs to AgNWPs. A higher magnification (Fig. 7 (Right)) shows the clear distribution of silver nanofillers in the composite foams. As for composite foams filled with AgNSs, the nanofillers were dispersed uniformly in the cell walls (Fig. 7 (Right)) and the ultra-thin cell membranes of the cellular structure (Fig. 7 (Left)). However, it can be clearly noticed that AgNSs appear to be insulating because the conductive particles surrounded by polymer resin could not touch one another. As for composite foams with AgNWs or AgNWPs, nanofillers were mainly dispersed in the struts and walls of the cellular structure and trace amounts of nanofillers were distributed in the ultra-thin cell membranes. The nanofillers in the cell walls adhered well to the polymer resin, indicating excellent resin permeability of the silver nanofillers/PIF due to the large surface area and the existence of interconnected cells. Moreover, the AgNWs oriented along the cell walls, possibly due to the strong stretching flow

generated during the cell growth. More specially, AgNWPs touched one another and formed a more compact packing structure due to the presence of silver nanoplatelets with large surface area on the AgNWs surface. In this case, AgNWs provided bridging effect for silver nanoplatelets, which promoted the effective connection between nanofillers.

To further clearly observe the distribution state of silver nanofillers in composite foams, PIF-P, PIF-W, and PIF-WS were subjected to chemical etching by NaOH and ethanol mixture for 5 h so that the polymer resin coated on the nanofillers was etched. Fig. 8 depicts the morphologies of cell walls for foams filled with silver nanofillers of different shapes after etching. Inset Fig. 8 (Right) shows the EDX spectures of the area scanning. General speaking, regardless of the nanofiller type, proper level of nanofiller dispersion could be noticed. The good dispersion of the nanofillers in the polymer can be mainly related to the processing method used to prepare the composite foam (in-situ polymerization and liquid foaming), the selection of a proper solvent (in this work DMF) to pre-disperse the nanofillers (ultrasonic dispersion), and the compatibility between the nanofillers (the coordination interaction of PVP on the surface) and the polyimide matrix. Compared to the composite foam filled with AgNSs without etching, the number of spheres appeared to be increased ascribed to the explosion of nanopheres buried in the polymer resin. However, it is still very difficult to observe networks of AgNSs aggregates in micrograph Fig.8 (PIF-P), due to the low aspect ratio of the aggregate, which was unfavourable for improving EMI shielding performance significantly. Micrographs Fig. 8 (PIF-W) and (PIF-WS) display, respectively, AgNWs and AgNWPs particles forming networks in the PIF matrix. As indicated in Fig. 8 (PIF-W), it can be clearly observed that the exposed AgNWs were deposited uniformly and densely in cell walls and intertwined with each other to form 3D network. In this case, a large number of connections between AgNWs tended to improve EMI shielding performance. With the addition of AgNWPs, a larger amount of nanofillers connections were densely dispersed in the matrix and constructed denser 3D networks due to AgNWs bridging effect, which would play a critical role in further enhancing EMI shielding

performance (Fig. 8 (PIF-WS)). In consideration of the 3D interconnected network structure of PIF, large 3D AgNWs networks or AgNWPs networks also existed in the whole foam, which would play an important part in improving the EMI shielding performance. The area scanning from the SEM-EDX profile of silver nanofillers/PIF confirmed that the major element was Ag due to the appearance of strong peaks at about 3 keV. The elements C and O should stem from the PIF matrix, and the Pt came from the spaying Pt in the testing process.

According to the FESEM micrographs, we conclude the schematic model of the silver nanofillers distribution in composite foams for PIF-P, PIF-W and PIF-WS, as shown in Fig. 9. Inset shows the 3D model of the distribution of silver nanofillers in composite foams. As for PIF-P, a large amount of AgNSs were deposited uniformly and densely on the cell walls and cell membranes. However, there were no connections between AgNSs, which were not effective for electromagnetic waves attenuation. As for PIF-W, interconnected AgNWs networks structure was formed in the cell walls and struts. Combined with the 3D AgNWs networks created by 3D structure of foams, the interconnected AgNWs networks in cell walls provided fast electron transport channels inside foams, which would be effective for electromagnetic waves attenuation. Therefore, such ultra-lightweight AgNWs/PI composite foams are expected to display a high EMI shielding performance. Compared to PIF-W, the growth of silver nanoplatelets on AgNWs in the polymer matrix promoted the formation of more surface connections or line connections between nanofillers due to the superior surface area and excellent mobility of silver nanoplatelets. Meanwhile, AgNWs provided bridging effect for the connection between nanoplatelets. This would be desirable for further improving the EMI shielding performance. Our data suggested that variation in nanofillers morphologies from nanospheres, nanowires to nanowires-nanoplates increased the number of connections between the nanofillers in the cell walls, thereby increasing the conductivity of networks. As a result, such ultra-lightweight silver nanofillers/PIF composites are an ideal material for blocking the unwanted electromagnetic waves because of the presence of highly interconnected conductive networks.

3.3 EMI shielding performance of silver nanofillers/polyimide composite foams

The severe electromagnetic radiation produced from modern electronics is very harmful to the human body, precision electronic equipment, and the environment. This is expressed as EMI, and should be blocked by using a shield. EMI SE is used to evaluate the material's ability to attenuate the electromagnetic wave strength, which is defined as the logarithmic ratio of incoming power (Pi) to transmitted power (Pt) of an electromagnetic wave and is expressed in dB. The higher the dB level of EMI SE, the more electromagnetic incident waves are blocked by the shielding material. Reflection loss (SE_R), absorption loss (SE_A), and multiple reflection loss (SE_M) are the three mechanisms of EMI SE, thus the total EMI SE is the sum of SE_R, SE_A and SE_M, as shown in Eq 1.[58-60]

$$\mathbf{SE_{total} = 10\,lg\frac{P_i}{P_t} = SE_R + SE_A + SE_M} \quad \textbf{(1)}$$

It is well known that the reflection loss originates from the mismatch of the intrinsic impedance between the shield and the air, the absorption loss results from the dissipative energy absorption of microwaves in the shield, and the multiple-reflection loss results from the internal non-uniformity of the shielding materials, which can be negligible when SE_{total} is high.[58] For plane wave radiation, SE_R and SE_A may also be calculated from the following equations[58-60]:

$$\mathbf{SE_A = 1.314d\sqrt{f\sigma_r\mu_r}} \quad \textbf{(2)}$$

$$\mathbf{SE_R = 168 - 10lg\frac{f\mu_r}{\sigma_r}} \quad \textbf{(3)}$$

where d is the shield thickness, σ_r is the electrical conductivity of the shield relative to pure copper, f is the frequency of electromagnetic wave, μ_r is the magnetic permeability of the shield relative to free space. It is evident that the absorption loss increases with the thickness, conductivity and frequency, while the reflection loss increases with increasing conductivity and decreases with the frequency.

Fig. 10 shows the EMI SE of composite foams filled with silver nanofillers in different morphologies at the same nanofiller loading measured in the frequency ranges of 30 MHz-1.5 GHz

and the X-band frequency ranges. A pure PIF without silver nanofillers was obviously transparent to electromagnetic waves and exhibited almost no shielding ability. The addition of silver nanofillers could improve the EMI SE. In the frequency ranges of 30 MHz-1.5 GHz, the EMI SE curves for PIF-P, PIF-W and PIF-WS were falling, an then tend to a stable level shown in Fig. 10a. For instance, for PIF-WS, the EMI SE decreased from 19 dB at 200 MHz to 8 dB at 1000 MHz, as shown in inset Fig. 10a. This phenomenon is consistent with the findings reported in the literature[45,59,60]. While, in the X-band frequency ranges, the EMI SE of all samples was found to be increased very slightly with the frequency. Importantly, it is notable that, at the same nanofiller loading, the EMI SE increased continuously with variation in silver nanofillers morphologies from nanospheres, nanowires to nanowires-nanoplatelets, possibly due to the variation in densities of interconnected nanofillers networks distributed in the foams. For example, the EMI SE increased from 14.5 dB for PIF-P to 19 dB for PIF-WS at 200 MHz, from 5 dB for PIF-P to 10 dB for PIF-WS at 600 MHz, from 2 dB for PIF-P to 8 dB for PIF-WS at 1000 MHz, and from 1.5 dB for PIF-P to 3.8 dB for PIF-WS at 9.6 GHz. Table 2 shows the volume conductivity of silver nanostructures/polyimide hybrid composite foams in this study. It was shown that the volume conductivity increased with the variation in silver nanofillers morphologies from nanospheres, nanowires to nanowires-nanoplatelets. It has been demonstrated that variation in nanofillers morphologies from AgNSs, AgNWs to AgNWPs increased the number of nanofillers connections, thereby increasing conductivity of networks. As given by Eq. (2) and Eq. (3), the EMI SE increased gradually.

In particular, the specific EMI SE, defined as the ratio of the SE to density, is a more appropriate criterion to compare the shielding performance between the silver nanofillers/PIF composite foams and other materials for applications that need lightweight materials. Fig. 11 displays the specific EMI SE silver nanofillers/PI composite foams measured in the frequency ranges of 30 MHz-1.5 GHz and the X-band frequency ranges. Inset shows their specific SE at 200 MHz, 600 MHz, 1000 MHz and 9.6 GHz. As shown in the Fig. 11a, the composite foam with AgNWPs exhibits the highest specific

SE among the three composite foams. Its specific SE was 1208 $dB \cdot g^{-1} \cdot cm^3$ at 200 MHz, 650 $dB \cdot g^{-1} \cdot cm^3$ at 600 MHz, and 488 $dB \cdot g^{-1} \cdot cm^3$ in the frequency range of 800-1500 MHz. These values are also much higher than those of typical shielding materials at the same frequency range previously reported in the literature. For instance, 15 $dB \cdot g^{-1} \cdot cm^3$ for polyethylene-carbon fiber composites with 20 wt% (11 vol%) carbon fiber loading,[61] 35.3 $dB \cdot g^{-1} \cdot cm^3$ for reduced graphene oxide (rGO)/epoxy composites containing 2 wt% rGO,[62] and 500 $dB \cdot g^{-1} \cdot cm^3$ graphene/polydimethylsiloxane (PDMS) foams with 0.8 wt% (about 0.037 vol %) graphene loading[63] were achieved at 30 MHz-1.5 GHz, respectively. In particular, the maximum specific SE of 216-249 $dB \cdot g^{-1} \cdot cm^3$ for PIF-WS at 8-12 GHz were achieved. These values are also superior to those of typical shielding materials at X-band frequency previously reported in the literature. For example, 64.4 $dB \cdot g^{-1} \cdot cm^3$ for PS/graphene foams with 30 wt% graphene loading,[13] 75 $dB \cdot g^{-1} \cdot cm^3$ for PI/graphene foam in 15 wt% graphene,[64] 42 $dB \cdot g^{-1} \cdot cm^3$ for PEI/graphene@Fe_3O_4 foam in 10 wt% graphene@Fe_3O_4 loading,[12] 33.1 $dB \cdot g^{-1} \cdot cm^3$ for PS/CNTs foam in 7 wt% CNTs,[65] 34 $dB \cdot g^{-1} \cdot cm^3$ for PP/carbon nanofiber in 10 vol% carbon nanofiber loading were achieved at 8-12 GHz, respectively.[66] Our data indicated that the good SE combined with ultralow density endowed the silver nanofillers/polyimide composite foam with a superior specific EMI SE, which is very desirable for applications that need lightweight materials. Moreover, AgNWPs/polymer composites exhibited superior specific EMI SE to the carbon-based polymer composites. This is considered to be due to the fact that AgNWPs interconnect with each other to form dense and interconnected network in polymer matrix due to its high aspect ratio and AgNWs bridging effects for silver nanoplatelets, which provided a fast electron transport pathway.

We also analyzed the EMI shielding mechanism of silver nanofillers/PI composite foams in this work. According to Eqs. (1), (2) and (3), for materials with high electrical conductivity, such as Ag, the main electromagnetic shielding mechanisms are reflection loss and absorption loss. Because of the limit of the measurement equipment, we only analyzed deeply the effectiveness contribution of different shielding mechanism at 8-12 GHz.[63] In the two-port network analysis system, the S_{11} (or S_{22})

and S_{21} (or S_{12}) parameters can be obtained, where the S_{11}, S_{21}, S_{12} and S_{22} generally stand for the forward refection coefficient, the forward transmission coefficient, the reverse transmission coefficient and the reverse refection coefficient, respectively.[9,67] SE can be evaluated based on scattering parameters using the following equation[3,8,9]:

$$\mathbf{SE_{total}} = -\mathbf{10log_{10}}|\boldsymbol{S_{12}}|^2 = -\mathbf{10log_{10}}|\boldsymbol{S_{21}}|^2 \quad \textbf{(4)}$$

Transmittance (T), reflectance (R), and absorbance (A) through the shielding material were analyzed by the S parameters, which can be described as follows[6, 67-70]:

$$\mathbf{T} = |\boldsymbol{S_{21}}|^2 = |\boldsymbol{S_{12}}|^2 \quad \textbf{(5)}$$

$$\mathbf{R} = |\boldsymbol{S_{11}}|^2 = |\boldsymbol{S_{22}}|^2 \quad \textbf{(6)}$$

$$\mathbf{A} + \mathbf{R} + \mathbf{T} = \mathbf{1} \quad \textbf{(7)}$$

The effective absorbance (A_{eff}) can be expressed as follows[6,67-72]:

$$\mathbf{A_{\boldsymbol{eff}}} = (\mathbf{1} - \boldsymbol{R} - \boldsymbol{T})/(\mathbf{1} - \mathbf{R}) \quad \textbf{(8)}$$

Considering the effective absorbance, A_{eff}, with respect to the power of the incident electromagnetic wave inside the shielding material, the refection loss and absorption loss can be expressed as follows [6, 67-73]:

$$\mathbf{SE_{\boldsymbol{R}}} = -\mathbf{10log_{10}}(\mathbf{1} - \mathbf{R}) = -\mathbf{10log_{10}}(\mathbf{1} - |\boldsymbol{S_{11}}|^2) \quad \textbf{(9)}$$

$$\mathbf{SE_{\boldsymbol{A}}} = -\mathbf{10log_{10}}\left[\frac{\mathbf{T}}{\mathbf{1-R}}\right] = -\mathbf{10log_{10}}\left[\frac{|\boldsymbol{S_{12}}|^2}{\mathbf{1}-|\boldsymbol{S_{11}}|^2}\right] \quad \textbf{(10)}$$

Fig. 12a displays the comparison of SE_A and SE_R of PIF-P, PIF-W and PIF-WS at 8-12 GHz, and their corresponding SE_{total}, SE_A and SE_R at 9.6 GHz is shown in Fig. 12b, which were calculated from the measured scattering parameters. It can be seen that both SE_A and SE_R increased with the variation in silver nanofillers from AgNSs, AgNWs, to AgNWPs. Moreover, it is worth noting that the contribution of SE_A to the SE_{total} is much larger than that of SE_R for all foams. For instance, at 9.6 GHz, SE_{total}, SE_A and SE_R are 3.9 dB, 3 dB and 0.9 dB for PIF-WS, respectively. And SE_{total}, SE_A and SE_R are 2.6 dB, 2.4 dB and 0.2 dB for PIF-W, respectively. Our data indicates that the silver

nanofillers/PI composite foams are both reflective and absorptive to electromagnetic wave in the X-band frequency range, and the absorption loss is the main attenuating mechanism.

The EMI SE measured in the frequency range of 30 MHz-1.5 GHz was used the standard coaxial cable method. In this measurement, we could not obtain the S_{11} and S_{21} parameters. Therefore, SE_R and SE_A at 30 MHz-1.5 GHz could not be calculated by the equations that showed the relationship between the parameters S_{12}, S_{11} and the reflection loss, the absorption loss. Moreover, it is worth noting that it is unreliable to calculate the SE_R and SE_A at 30 MHz-1.5 GHz for composite foams according to the Eqs. (2) and (3).[58,74] Actually, Eqs. (2) and (3) are developed for conductive monolithic materials,[58] and they are not completely suitable for shielding material with a composite foam structure filled with silver nanofillers. The possible reasons are as follows: on one hand, the constriction resistance and high current dissipation at the nanofiller contact points existed[58]; on the other hand, the cell structure have effects on the dissipation of unwanted electromagnetic waves.[75] Despite the unreliable EMI SE predictions made by Eqs. (2) and (3), these two equations can be used as criterions to anticipate the general effects of different parameters on the EMI SE at 30 MHz-1.5 GHz. According to Eqs. (2) and (3), reflection loss decreases with increasing frequency, while absorption loss increases with increasing frequency.[59,60] The EMI SE for all studied samples decreases as increasing frequency until about 800 MHz, and then nearly reaches a plateau, indicating that reflections loss may be the major contribution to EMI shielding at 30-800 MHz, and the composite foams are both reflective and absorptive to electromagnetic radiation at 800 MHz-1.5GHz.

Fig. 13 shows the schematic description of electromagnetic microwave dissipation in the silver nanofillers/PI composite foams for PIF-P, PIF-W and PIF-WS. As for PIF-P, due to the absence of interconnected conductive network, most of the incident electromagnetic microwaves can easily pass through the composite foam with less reflectivity (Fig. 13 (PIF-P)). As for PIF-W and PIF-WS, interconnected AgNWs network or AgNWPs network in the cell walls combined with the 3D

AgNWs network or AgNWPs network network formed by copying the structure of the whole foam could provide fast electronic channels inside the foam, leading to the electromagnetic microwave dissipation. In this case, the presence of cells created a huge gaseous cell-polymer matrix interface area and the large aspect ratio of silver nanofillers also induced a large AgNWs-polymer resin interface area. The incident electromagnetic waves would be repeatedly reflected and scattered at these interfaces numerous times and they were difficult to escape from the foams before being dissipated as heat. In particular, the presence of AgNWs bridging effects in PIF-WS enhanced the AgNWPs network density, thereby increasing the conductivity and EMI shielding properties. In brief, the reflections of interconnected AgNWs or AgNWPs networks inside the shield combined with the absorptions resulting from the multiple reflections at interfaces inside the shield contributed to the shielding effect.

4. Conclusions

We have developed a facile two-step method to fabricate AgNWPs using AgNWs as seeds. The in-situ growth mechanism of silver nanoplatelets on AgNWs surface was demonstrated. The morphology and the EMI SE of AgNSs, AgNWs or AgNWPs hybrid polyimide composite foams at 30 MHz-1.5 GHz and 8-12 GHz were studied to reveal the effect of nanofiller type on the cell morphology and EMI shielding properties, to analyze the EMI shielding mechanism. Based on the experimental results, the following conclusions can be drawn:

(1) 0.45 M $AgNO_3$ concentration was the appropriate condition for the in-situ growth of AgNPs on AgNWs to produce AgNWPs at 3 mM AgNWs concentration. The difference in favorable planes in EG and DMF of selective adsorption of PVP resulted in the shape evolution.

(2) The as-prepared composite foams exhibited low density of 0.014-0.017 g/cm^3 and microcellular structure with average diameter of 166-426 μm. And the open cell content was found to be 94.6% ~ 89.2%. AgNWs and AgNWPs were deposited uniformly and densely on the cell walls, while AgNSs were distributed in cell walls and membranes.

(3) AgNWPs/PIF composite foam exhibited outstanding EMI SE compared to those of AgNSs/PIF and AgNWs/PIF at the same nanofiller loading. For example, at nanofiller loading of 4.5 wt%, a minimum EMI SE of 30-2.5 dB at 30 MHz-1.5 GHz and 1.4 dB at 8 -12 GHz for AgNSs/PIF were achieved because there were no connections between AgNSs in cell walls; a better EMI SE of 35-6 dB at 30 MHz-1.5 GHz and 2.5-3.2 dB at 8 -12 GHz for AgNWs/PIF were achieved due to the dense AgNWs network in cell walls; a maximum EMI SE of 35-8 dB at 30 MHz-1.5 GHz and 3.8-5 dB at 8-12 GHz for AgNWPs/PIF were achieved owing to the denser interconnected AgNWPs networks by introducing AgNWs bridging effects for silver nanoplatelets. More importantly, combined with ultralow density, this caused outstanding specific EMI SE like 1208 $dB \cdot g^{-1} \cdot cm^3$ at 200 MHz, 216-249 $dB \cdot g^{-1} \cdot cm^3$ at 8-12 GHz, which far surpasses the best values of other composite materials.

(4) The reflections of interconnected AgNWs or AgNWPs networks inside the shield combined with the absorptions resulting from the multiple reflections at interfaces inside the shield contributed to the shielding effect. While, regardless of the nanofiller type, absorptions were higher than reflections at 8-12 GHz, suggesting that absorptions are the main shielding mechanism in the X band.

Our data demonstrates that AgNWPs/polyimide composite foams can be used as a lightweight and high-performance EMI shielding material against electromagnetic pollution, especially for advanced applications in the aircraft and spacecraft fields.

Notes and references

1 W. L. Song, X. T. Guan, L. Z. Fan, W. Q. Cao, C. Y. Wang, Q. L. Zhao and M. S. Cao, *J. Mater. Chem. A,* 2015, **3**, 2097-2107.

2 D. Micheli, R. B. Morles, M. Marchetti, F. Moglie and V. M. Primiani, *Carbon*, 2014, **68**, 149-158.

3 S. Kim, J. S. Oh, M. G. Kim, W. Jang, M. Wang, Y. Kim, H. W. Seo, Y. C. Kim, J. Lee, Y. Lee, and J. Nam, *ACS Appl. Mater. Interfaces*, 2014, **6**, 17647-17653.

4 B. Shen, W. T. Zhai and W. G. Zheng, *Adv. Funct. Mater.*, 2014, **24,** 4542-4548.

5 S. Maiti, N. K. Shrivastava, S. Suin and B. B. Khatua, *ACS Appl. Mater. Interfaces*, 2013, **5**, 4712-4724.

6 W. L. Song, J. Wang, L. Z. Fan, Y. Li, C. Y. Wang and M. S. Cao, *ACS Appl. Mater. Interfaces*, 2014, **6**, 10516-10523.

7 Y. Yang, M. C. Gupta, K. L. Dudley and R. W. Lawrence, *Adv. Mater.*, 2005, **17**, 1999-2003.

8 G. P. Kar, S. Biswas, R. Rohini and S. Bose, *J. Mater. Chem. A*, 2015, **3**, 7974-7985.

9 S. P. Pawar, D. A. Marathe, K. Pattabhi and S. Bose, *J. Mater. Chem. A,* 2015, **3**, 656-669.

10 H. D. Huang, C. Y. Liu, D. Zhou, X. Jiang, G. J. Zhong, D. X. Yan and Z. M. Li, *J. Mater. Chem. A,* 2015, **3**, 4983-4991.

11 Y. Chen, Y. Wang, H. B. Zhang, X. Li, C. X. Gui and Z. Z. Yu, *Carbon*, 2015, **82**, 67-76.

12 B. Shen, W. T. Zhai, M. Tao, J. Ling and W. G. Zheng, *ACS Appl. Mater. Interfaces*, 2013, **5**, 11383-11387.

13 D. X. Yan, P. G. Ren, H. Pang, Q. Fu, M. B. Yang and Z. M. Li, *J. Mater. Chem.*, 2012, **22**, 18772-18774.

14 H. B. Zhang, Q. Yan, W. G. Zheng, Z. He and Z. Z. Yu, *ACS Appl. Mater. Interfaces*, 2011, **3**, 918-924.

15 J. Q. Ling, W. T. Zhai, W. Feng, J. F. Zhang and W. G. Zheng, *ACS Appl. Mater. Interfaces*, 2013, **5**, 2677-268.

16 A. Ameli, M. Nofar, S. Wang and C. B. Park, *ACS Appl. Mater. Interfaces*, 2014, **6**, 11091-11100.

17 G. A. Gelves, M. H. Al-Saleh and U. Sundararaj, *J. Mater. Chem.*, 2011, **21**, 829–836.

18 M. J. Hu, J. F. Gao,, Y. C. Dong, K. Li, G. C. Shan, S. L. Yang and R. K. Y. Li, *Langmuir*, 2012, **28**, 7101-7106.

19 Y. H. Yu, C. C. M. Ma, C. C. Teng, Y. L. Huang, S. H. Lee, I. Wang and M. H. Wei, *Mater. Chem. Phys.*, 2012, **136**, 334-340.

20 S. Kwon, R. Ma, U. Kim, H. R. Choi and S. Baik, *Carbon*, 2014, **68**, 118-124.

21 M. H. Al-Saleh, W. H. Saadeh and U. Sundararaj, *Carbon*, 2013, **60**, 146-156.

22 M. M. Bernal, M. Mario-Gallego, I. Molenberg, I. Huynen, M. A. L. Manchado and R. Verdejo, *RSC Adv.*, 2014, **4**, 7911-7918.

23 Y. Yang, M. C. Gupta, K. L. Dudley and R. W. Lawrence, *J. Nanosci. Nanotechnol.*, 2005, **5**, 927-931.

24 W. Shen, X. Zhang, Q. Xu and W. Song, *Nanoscale*, 2014, **6**, 1622-1628.

25 M. Tsuji, Y. Maeda, S. Hikino, H. Kumagae, M. Matsunaga, R. Matsuo, X. L. Tang, M. Ogino and P. Jiang, *Cryst. Growth Des*., 2009, **9**, 4700-4705.

26 S. Coskun, B. Aksoy and H. E. Unalan, *Cryst. Growth Des.*, 2011, **11**, 4963-4969.

27 C. C. S. Oliveira, R. A. Ando and P. H. C. Camargo, *Phys. Chem. Chem. Phys.*, 2013, **15**, 1887-1893.

28 J. Perelaer, R. Abbel, S. Wünscher , R. Jani, T. Lammeren and U. S. Schubert, *Adv. Mater.*, 2012, **24**, 2620-2625.

29 H. Jiang, K. Moon, J. Lu and C. P. Wong, *J. Electron. Mater.*, 2005, **34**, 1432-1439.

30 R. Zhang, W. Lin, K. Moon and C. P. Wong, *ACS Appl. Mater. Interfaces*, 2010, **5**, 2637-2645.

31 R. Zhang, K. Moon, W. Lin and C. P. Wong, *J. Mater. Chem.*, 2010, **20**, 2018-2023.

32 Y. Atwa, N. Maheshwari and I. A. Goldthorpe, *J. Mater. Chem. C*, 2015, **3**, 3908-3912.

33 M. Sureshkumar, H. Y. Na, K. H. Ahn and S. J. Lee, *ACS Appl. Mater. Interfaces*, 2015, **7**, 756-764.

34 A. Lonjon, I. Caffrey, D. Carponcin, E. Dantras and C. Lacabanne. *J. Non-Cryst. Solids*, 2013, **376**, 199-204.

35 G. A. Gelves, B. Lin, U. Sundararaj and J. A. Haber, *Adv. Funct. Mater.*, 2006, **16**, 2423-2430.

36 T. H. L. Nguyen, L. Q. Cortes, A. Lonjon, E. Dantras and C. Lacabanne, *J. Non-Cryst. Solids*, 2014, **385**, 34-39.

37 H. O. Choi, D. W. Kim, S. J. Kim, K. M. Cho and H. T. Jung, *J. Mater. Chem. C*, 2014, **2**, 5902-5909.

38 A. A. Al-Ghamdi, O. A. Al-Hartomy, F. El-Tantawy and F. Yakuphanoglu, *Microsyst. Technol*. 2014, 1-10.

39 Y. Hu, H. Zhang, F. Li, X. Cheng and T. Chen, *Polym. Test.*, 2010, **29**, 609-612.

40 G. Harikrishnan, S. N. Singh, E. Kiesel and C. W. Macosko, *Polymer*, 2010, **51**, 3349-3353.

41 X. Y. Liu, M. S. Zhan, K. Wang, Y. Li and Y. F. Bai, *Polym. Adv. Technol.*, 2012, **23**, 677-685.

42 X. Y. Liu, M. S. Zhan and K. Wang, *J. Appl. Polym. Sci.*, 2013, **127**, 4129-4137.

43 J. J. Ma, M. S. Zhan and K. Wang, *J. Appl. Polym. Sci.*, 2014, **131**, 39881.

44 M. B. Saeed and M. S. Zhan, *Int. J. Adhes. Adhes.*, 2007, **27**, 9-19.

45 J. J. Ma, M. S. Zhan and K. Wang, *ACS Appl. Mater. Interfaces*, 2014, **7**, 563-576.

46 J. J. Ma, M. S. Zhan, *RSC adv.*, 2014, **4**, 21060-21071.

47 X. H. Chen, L. Z. Liu, J. Liu, F. S. Pan, *Acta Metall. Sin. (Engl. Lett.)*, 2015, **28**, 492-498.

48 A. Amarjargal, L. D. Tijing, I. T. Im and C. S. Kim, *Chem. Eng. J.,* 2013, **226**, 243-254.

49 J. Mu, B. Chen, Z. Guo, M. Zhang, Z. Zhang, P. Zhang, C. Shao and Y. Liu, *Nanoscale*, 2011, **3**, 5034-5040.

50 M. Tsuji, X. Tang, M. Matsunaga, Y. Maeda and M. Watanabe, *Cryst. Growth Des*., 2010, **10**, 5238-5243.

51 B. Wiley, Y. Sun, B. Mayers and Y. Xia, *Chem. Eur. J.*, 2005**, 11**, 454-463.

52 X. Cao, L. L. James, T. Widya and C. Macosko, *Polymer*, 2005, **46**, 775-783.

53 Y. Li, Ragauskas and A. J. Ethanol, *RSC Adv.*, 2012, ***2***, 3347-3351.

54 L. Madaleno, R. Pyrz, A. Crosky, L. R. Jensen, J. C. M. Rauhe, V. Dolomanova, A. M. V. B. Timmons, J. J. C. Pinto and J. Norman, *Compos. Part A*, 2013*,* **44**, 1-7.

55 S. Pardo-Alonso, E. Solórzano, S. Estravís, M. A. Rodríguez-Perez and J. A. de Saja, *Soft Matter*, 2012, **8**, 11262-11270.

56 M. M. Bernala, S. Pardo-Alonso, E. Solórzano, M. A. Lopez-Manchadoa, R. Verdejo and M. A. Rodríguez-Perez, *RSC Adv.*, 2014, **4**, 20761-20768.

57 G. Harikrishnan, C. I. Lindsay, M. A. Arunagirinathan and C. W. Macosko, *ACS Appl. Mater. Interfaces*, 2009, **1,** 1913-1918.

58 K. J. Ji, H. H. Zhao, J. Zhang, J. Chen and Z. D. Dai, *Appl. Surf. Sci.*, 2014, **311**, 351-356.

59 X. H. Chen, L. Z. Liu, F. S. Pan, J. J. Mao, X. Y. Xu and T. Yan, *Mat. Sci. Eng. B*, 2015, 197, 67-74.

60 X. H. Chen, J. Liu, Z. H. Zhang and F. S. Pan, *Mater. Design*, 2012, 42, 327-333.

61 B. S. Villacorta, A. A. Ogale and T. H. Hubing, *Polym. Eng. Sci.*, 2013**, 53**, 417-423.

62 N. Yousefi, X. Sun, X. Lin, X. Shen, J. Jia, B. Zhang, B. Tang, M. Chan and J. K. Kim, *Adv. Mater.*, 2014, **26**, 5480-5487.

63 Z. P. Chen, C. Xu, C. Q. Ma, W. C. Ren and H. M. Cheng, *Adv. Mater.*, 2013, ***25***, 1296-1300.

64 Y. Li, X. Pei, B. Shen, W. Zhai, L. Zhang and W. Zheng, *RSC Adv.*, 2015, **5**, 24342-24351.

65 Y. Yang and M. C. Gupta, *Nano Lett.*, 2005, **5,** 2131-2134.

66 A. Ameli, P. U. Jung and C. B. Park, *Carbon*, 2013, **60**, 379-391.

67 S. T. Hsiao, C. C. M. Ma, W. Liao, Y. S. Wang, S. M. Li, Y. C. Huang, R. B. Yang and W. F. Liang, *ACS Appl. Mater. Interfaces*, 2014, **6**, 10667-10678.

68 S. T. Hsiao, C. C. M. Ma, H. W. Tien, W. H. Liao, Y. S. Wang, S. M. Li, C. Y. Yang, S. C. Lin and R. B. Yang, *ACS Appl. Mater. Interfaces*, 2015, 7, 2817-2826.

69 S. Maiti, S. Suin, N. K. Shrivastava and B. B. Khatua, *RSC Adv.*, 2014, **4**, 7979-7990.

70 W. L. Song, L. Z. Fan, M. S. Cao, M. M. Lu, C.Y. Wang, J. Wang, T. T. Chen, Y. Li, Z. L. Hou, J. Liu and Y. P. Sun, *J. Mater. Chem. C,* 2014, **2**, 5057-5064.

71 H. R. Kim, B. S. Kim and I. S. Kim, *Mater. Chem. Phys.*, 2012, **135**, 1024-1029.

72 K. Yao, J. Gong, N. Tian, Y. Lin, X. Wen, Z. Jiang, H. Na and T. Tang, *RSC Adv.,* 2015, 5, 31910-31919.

73 M. Sharma, M. P. Singh, C. Srivastava, G. Madras, and S. Bose, *ACS Appl. Mater. Interfaces,* 2014, 6, 21151-21160.

74 M. H. Al-Saleh, U. Sundararaj, *J. Phys. D: Appl. Phys.*, 2013, 46, 35304.

75 S. R. Dhakate, K. M. Subhedar and B. P. Singh, *RSC Adv.*, 2015, **5**, 43036-43057.

Tables and captions

Table 1 Density, nanofiller loading, and morphological properties of silver nanostructures/polyimide hybrid composite foams in this study.

Sample	PIF-0	PIF-P	PIF-W	PIF-WS
Silver nanostructures content in foams (wt%)	0	4.5	4.5	4.5
Apparent viscosity (mPa·s)	489	1692	924	976
Maximum cell size (μm)	631	426	655	568
Minimum cell size (μm)	273	82	255	345
Average cell diameter (μm)	397±86	166±128	434±106	426±86
Open cell content (%)	94.6±0.8	92.5±0.4	89.2±0.3	90.6±0.3
Foam density(g/cm^3)	0.014±0.001	0.015±0.003	0.017±0.002	0.016±0.004

Table 2 Volume conductivity of silver nanostructures/polyimide hybrid composite foams in this study.

Sample	PIF-0	PIF-P	PIF-W	PIF-WS
Volume conductivity (S/m)	1.3×10^{-14}	2.1×10^{-10}	5.4×10^{-8}	3.2×10^{-7}

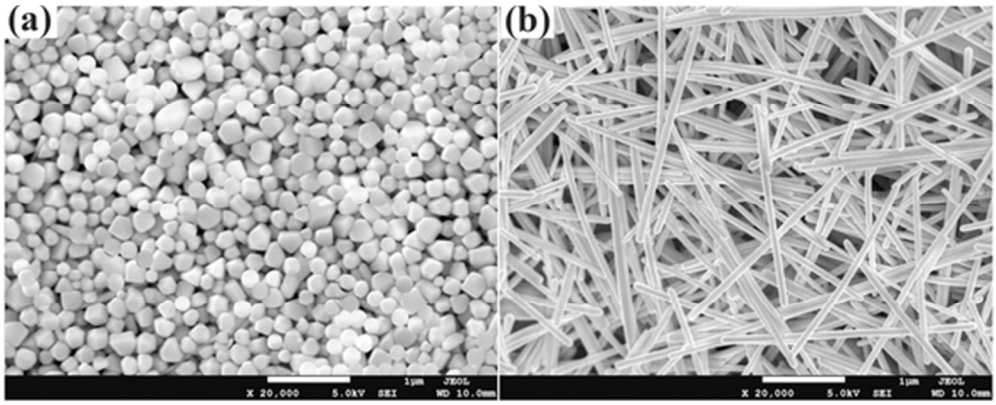

Fig. 1 FESEM images of the as-synthesized silver nanostrctures: (a) AgNSs, (b) AgNWs.
25x10mm (600 x 600 DPI)

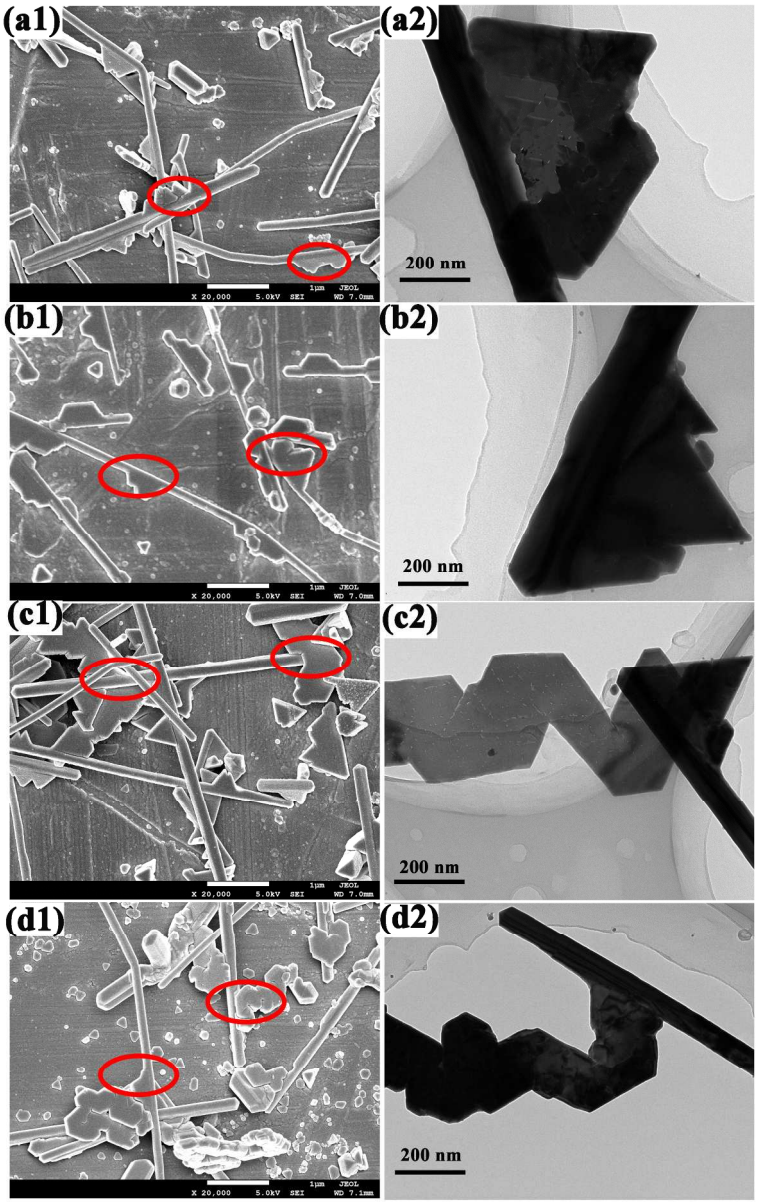

Fig. 2 FESEM images (Left) and TEM images (Right) of AgNWPs synthesized at various AgNO3 concentration: (a1, a2) 0.15 M; (b1, b2) 0.30 M; (c1, c2) 0.45 M; (d1, d2) 0.60 M.
100x158mm (600 x 600 DPI)

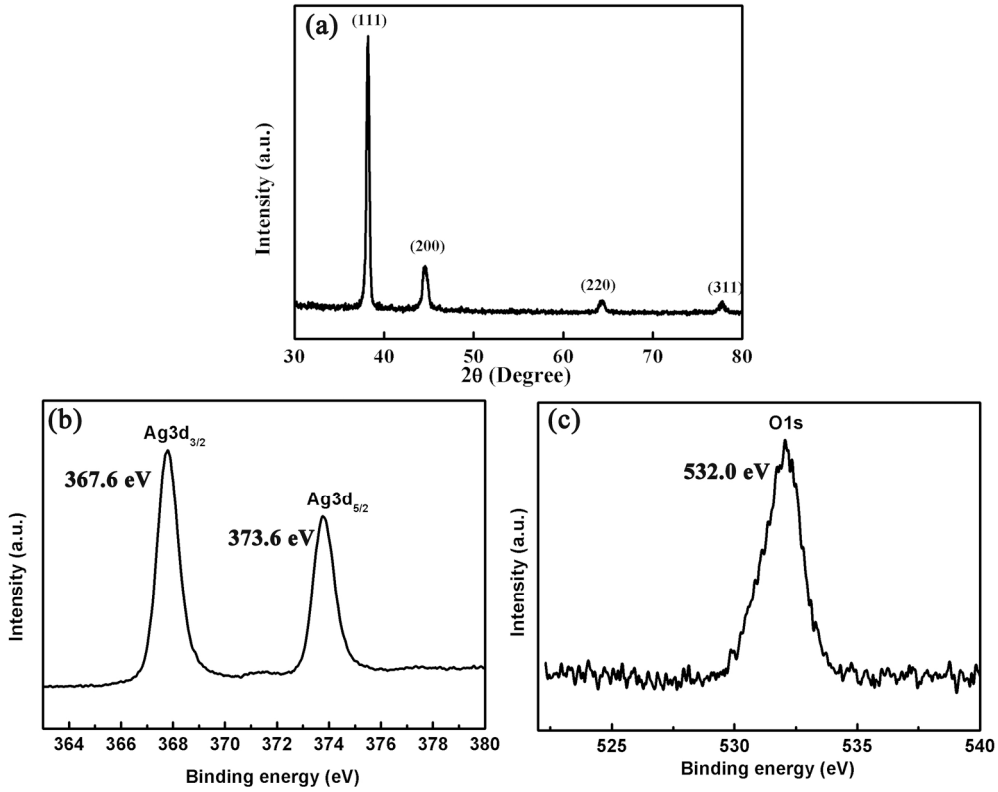

Fig. 3 XRD of AgNWPs (a); XPS spectra of AgNWPs: (b) Ag 3d spectrum, (c) O 1s spectrum.
100x79mm (600 x 600 DPI)

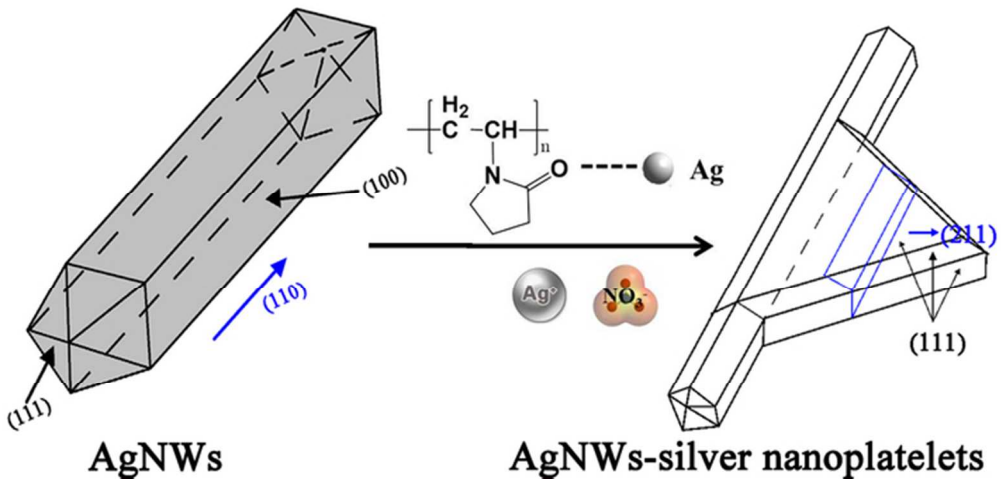

Fig. 4 In-situ growth mechanism of the silver nanoplatelets on the AgNWs surface.
30x14mm (600 x 600 DPI)

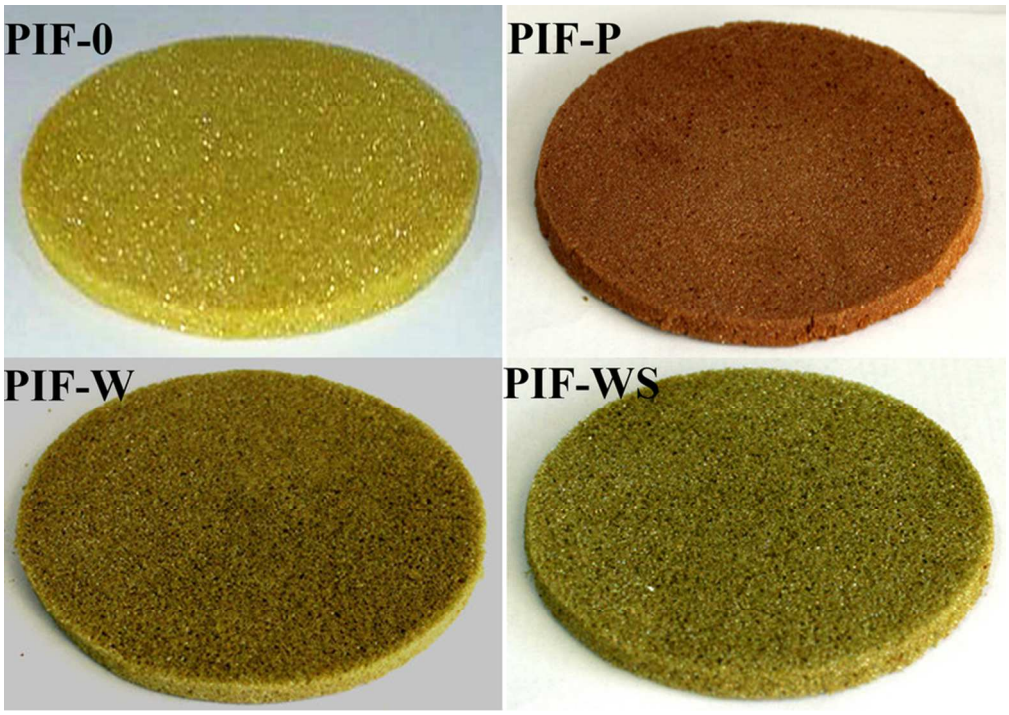

Fig. 5 Photographs of composite foams for PIF-0, PIF-P, PIF-W, and PIF-WP.
44x31mm (600 x 600 DPI)

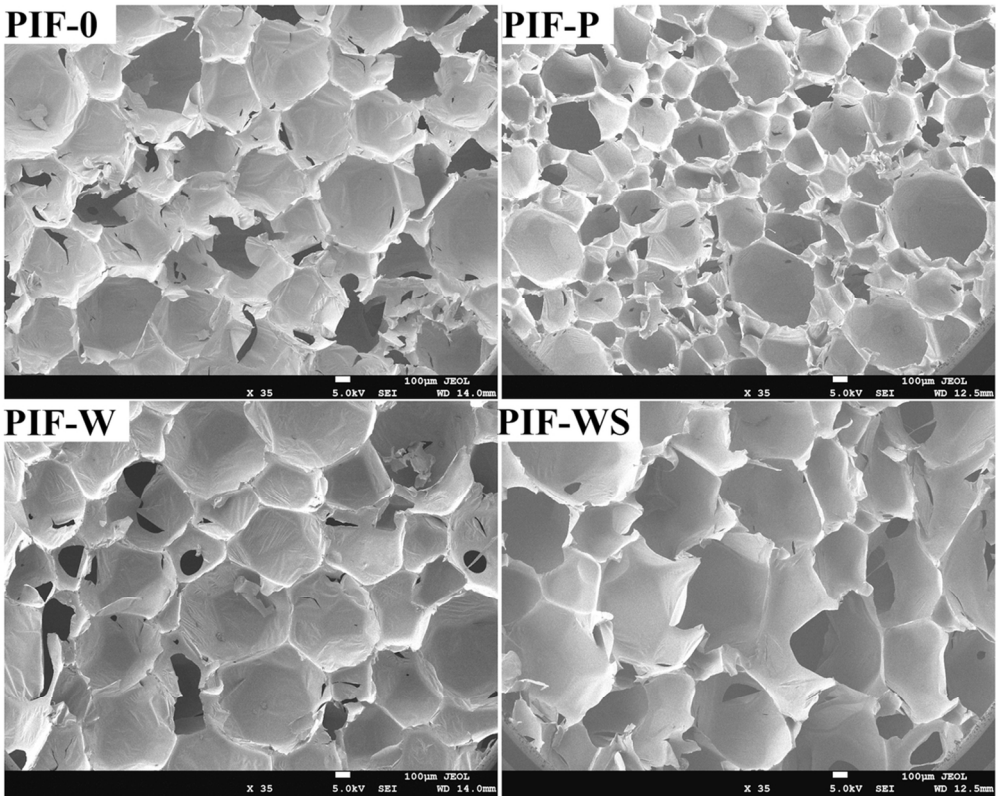

Fig. 6 FESEM micrographs of silver nanofillers/PI composite foams: (PIF-0) pure PIF; (PIF-P) AgNSs/PI composite foams; (PIF-W) AgNWs/PI composite foams; (PIF-WS) AgNWPs/PI composite foams.
50x40mm (600 x 600 DPI)

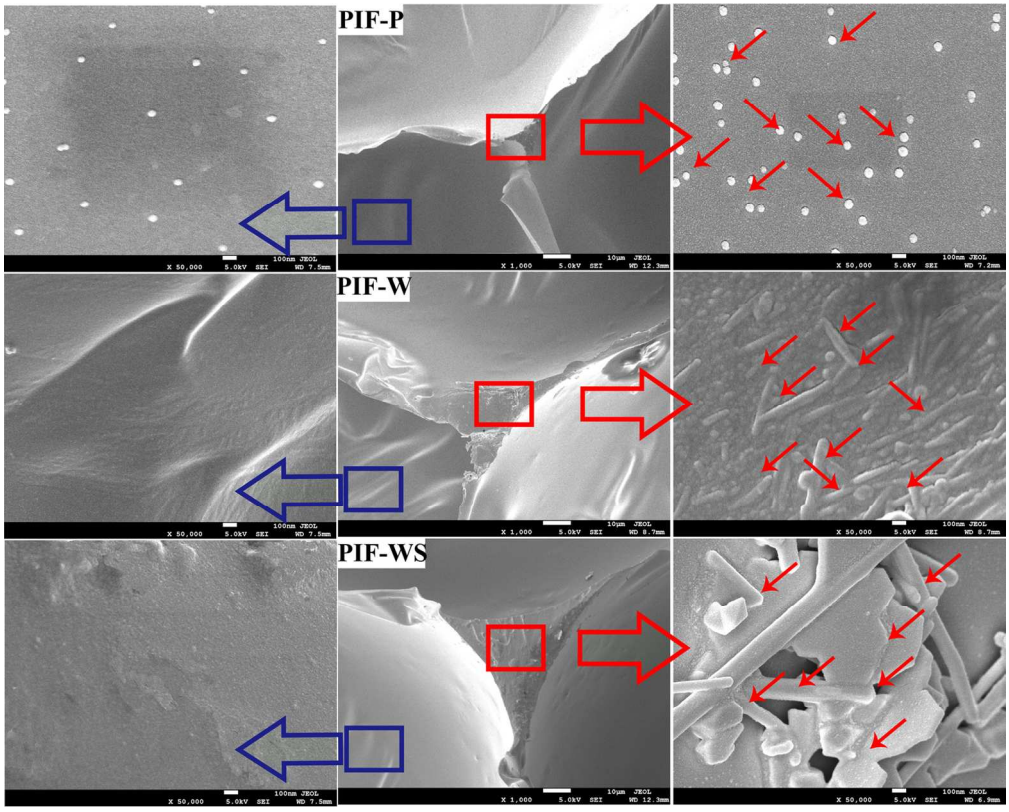

Fig. 7 Dispersion of silver nanostructures in composite foams for PIF-P, PIF-W and PIF-WS: (Middle) FESEM images of cell walls; (Left) FESEM images of the distribution of silver nanostructures in cell membranes; (Right) FESEM images of the distribution of silver nanostructures in cell walls.
67x54mm (600 x 600 DPI)

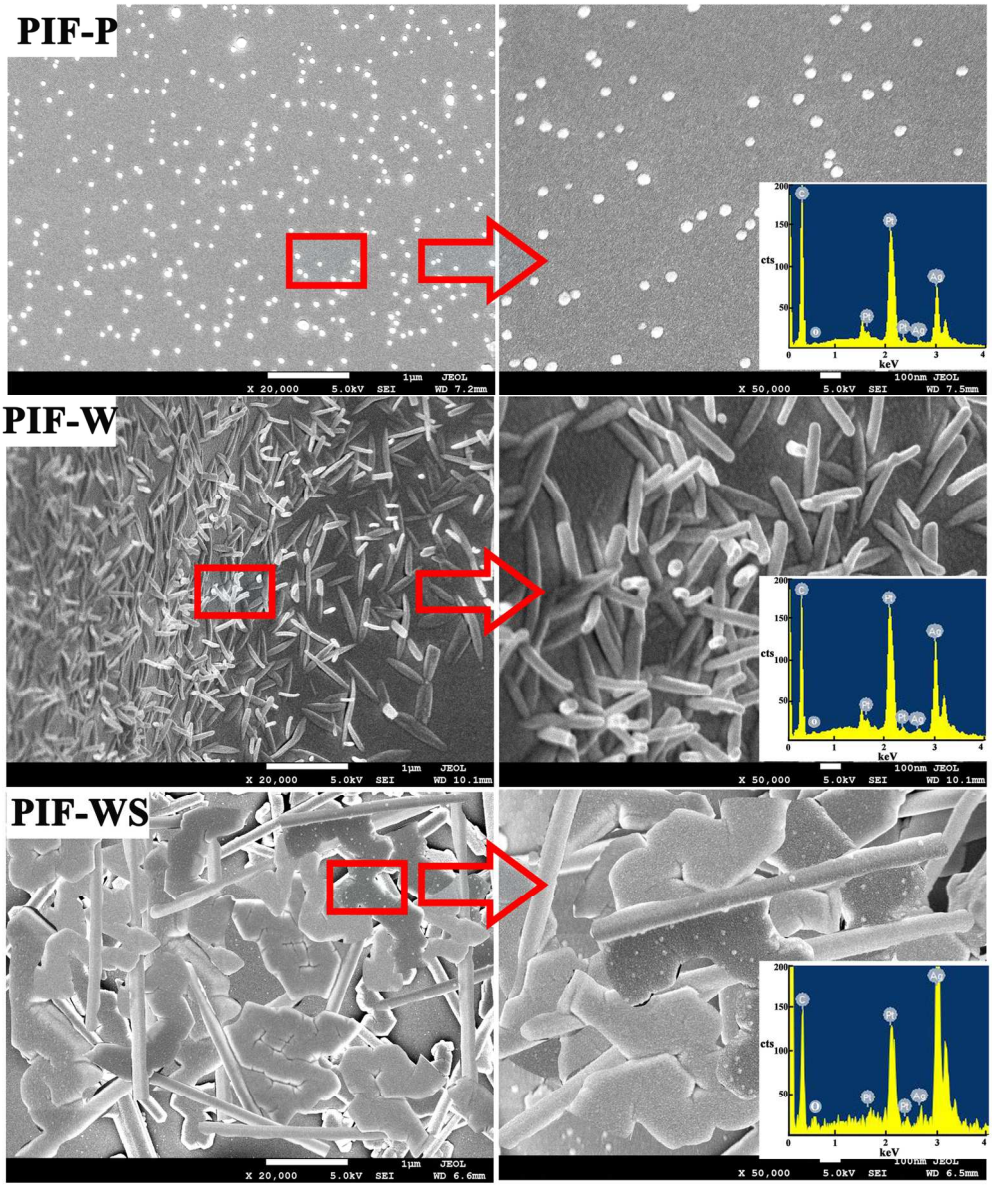

Fig. 8 FESEM images of the distribution of silver nanostructures in composite foams for PIF-P, PIF-W and PIF-WS after etching: (Left) low magnification (20k); (Right) high magnification (50k). Inset (Right) shows the EDS images of area scanning.
76x91mm (600 x 600 DPI)

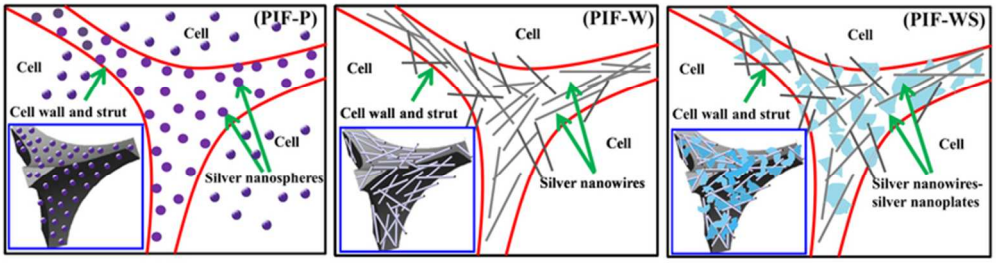

Fig. 9 Schematic model of the distribution of silver nanostructures in composite foams for PIF-P, PIF-W and PIF-WS. Inset shows the 3D model of the distribution of silver nanofillers in composite foams.
33x8mm (600 x 600 DPI)

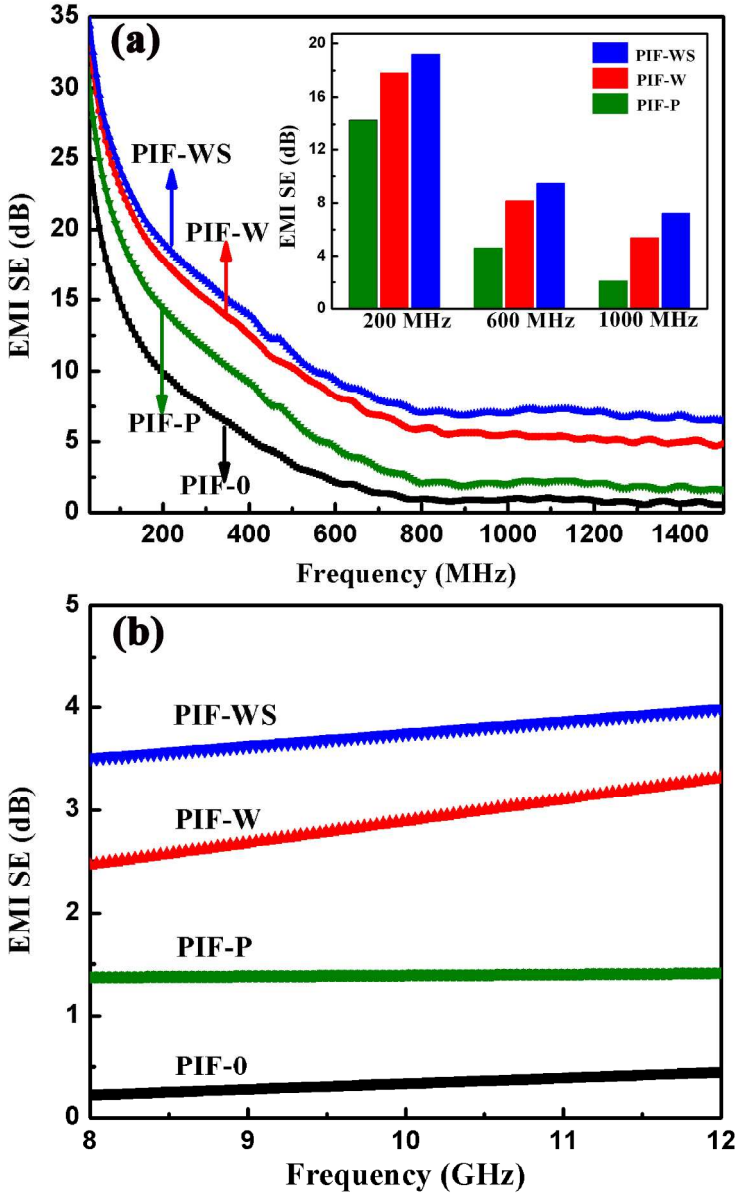

Fig. 10 EMI SE of composite foams for PIF-0, PIF-P, PIF-W and PIF-WS measured in frequency ranges (a) 30 MHz-1.5 GHz, and (b) 8-12 GHz. Inset (a) shows their EMI SE at 200 MHz, 600 MHz, and 1000 MHz.
137x222mm (600 x 600 DPI)

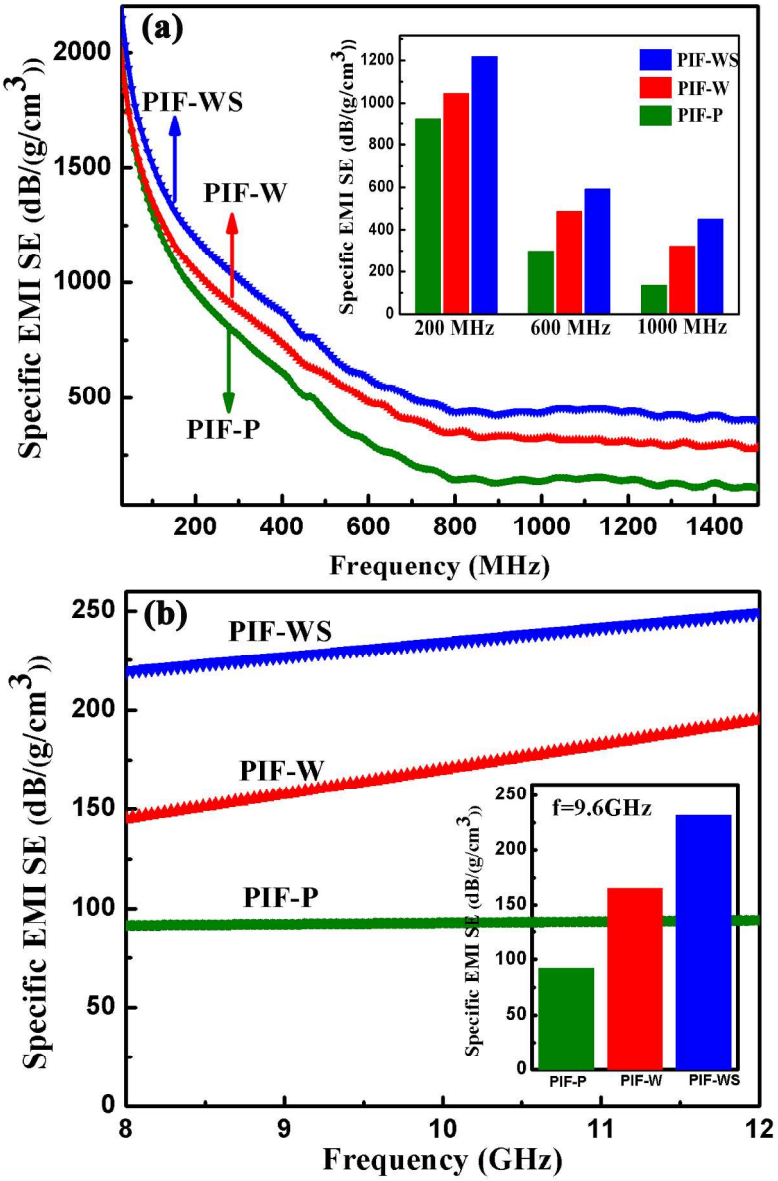

Fig. 11 Specific EMI SE of composite foams for PIF-P, PIF-W and PIF-WS measured in frequency ranges (a) 30 MHz-1.5 GHz, and (b) 8-12 GHz. Inset (a) shows their specific EMI SE at 200 MHz, 600 MHz, and 1000 MHz. Inset b shows the specific EMI SE of composite foams at 9.6 GHz.
130x200mm (600 x 600 DPI)

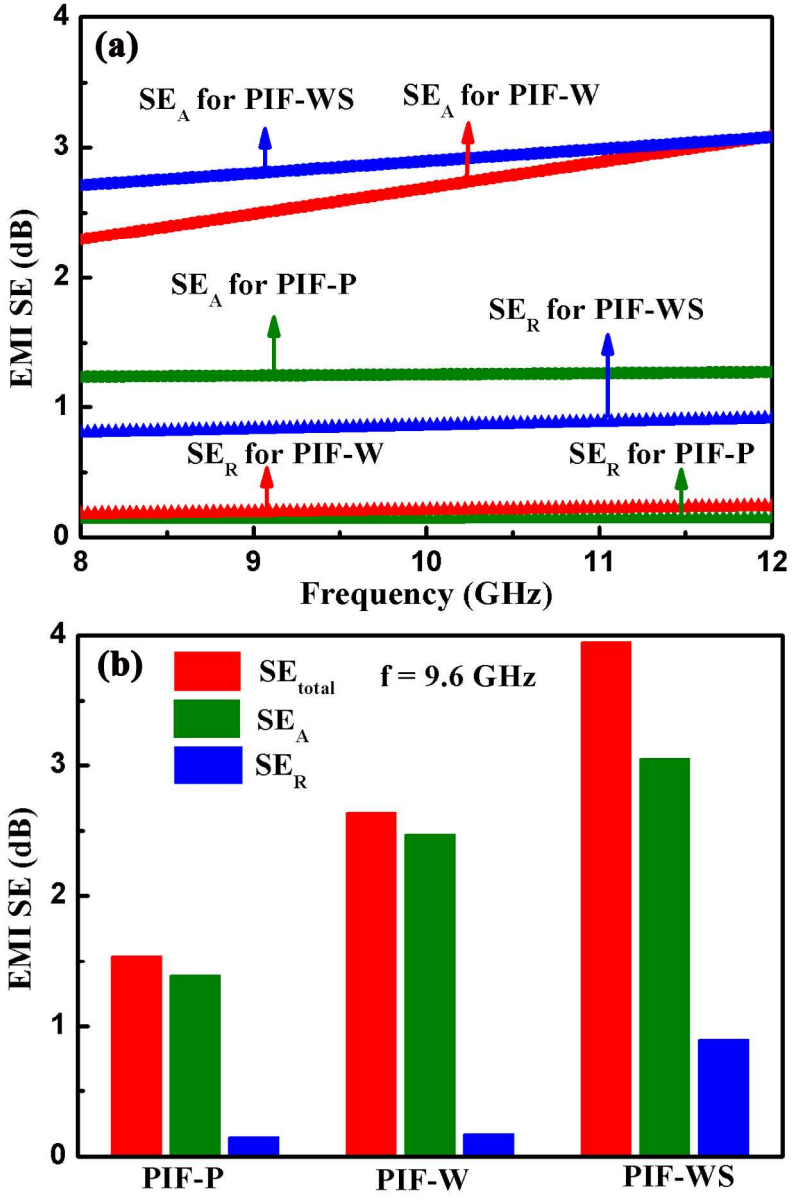

Fig. 12 (a) Comparison of SEA and SER of composite foams for PIF-P, PIF-W and PIF-WS at 8-12 GHz. (b) The corresponding SEtotal, SEA and SER at 9.6 GHz.
126x187mm (600 x 600 DPI)

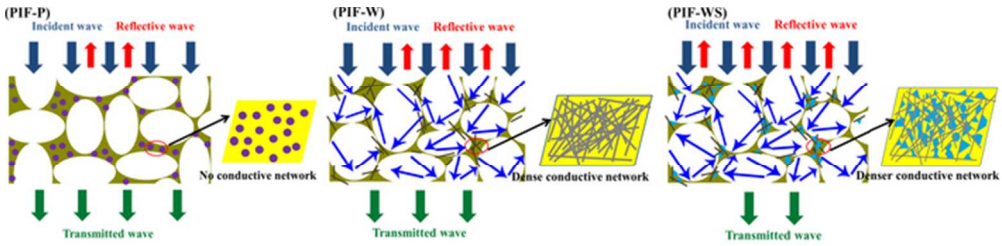

Fig. 13 Schematic description of electromagnetic wave transfer across the composite foams for PIF-P, PIF-W and PIF-WS.
30x7mm (600 x 600 DPI)